BIOCHEMISTRY
including biophysical chemistry & molecular biology

Article

pubs.acs.org/biochemistry

Molecular Mechanisms of Inhibition of Influenza by Surfactant Protein D Revealed by Large-Scale Molecular Dynamics Simulation

Boon Chong Goh,[†] Michael J. Rynkiewicz,[‡] Tanya R. Cafarella,[‡] Mitchell R. White,[§] Kevan L. Hartshorn,[§] Kimberly Allen,[∥] Erika C. Crouch,[∥] Oliviana Calin,[⊥] Peter H. Seeberger,[⊥] Klaus Schulten,*[,†] and Barbara A. Seaton*[,‡]

[†]Beckman Institute and Department of Physics, University of Illinois at Urbana-Champaign, Urbana, Illinois 61801, United States

[‡]Department of Physiology and Biophysics and [§]Department of Medicine, Boston University School of Medicine, Boston, Massachusetts 02118, United States

[∥]Department of Pathology and Immunology, Washington University School of Medicine, St. Louis, Missouri 63110, United States

[⊥]Department of Biomolecular Systems, Max-Planck-Institute of Colloids and Interfaces, 14476 Potsdam, Germany, and Institute for Chemistry and Biochemistry, Freie Universität, 14195 Berlin, Germany

Supporting Information

ABSTRACT: Surfactant protein D (SP-D), a mammalian C-type lectin, is the primary innate inhibitor of influenza A virus (IAV) in the lung. Interactions of SP-D with highly branched viral N-linked glycans on hemagglutinin (HA), an abundant IAV envelope protein and critical virulence factor, promote viral aggregation and neutralization through as yet unknown molecular mechanisms. Two truncated human SP-D forms, wild-type (WT) and double mutant D325A+R343V, representing neck and carbohydrate recognition domains are compared in this study. Whereas both WT and D325A +R343V bind to isolated glycosylated HA, WT does not inhibit IAV in neutralization assays; in contrast, D325A +R343V neutralization compares well with that of full-length native SP-D. To elucidate the mechanism for these biochemical observations, we have determined crystal structures of D325A +R343V in the presence and absence of a viral nonamannoside (Man9). On the basis of the D325A+R343V−Man9 structure and other crystallographic data, models of complexes between HA and WT or D325A+R343V were produced and subjected to molecular dynamics. Simulations reveal that whereas WT and D325A+R343V both block the sialic acid receptor site of HA, the D325A+R343V complex is more stable, with stronger binding caused by additional hydrogen bonds and hydrophobic interactions with HA residues. Furthermore, the blocking mechanism of HA differs for WT and D325A+R343V because of alternate glycan binding modes. The combined results suggest a mechanism through which the mode of SP-D−HA interaction could significantly influence viral aggregation and neutralization. These studies provide the first atomic-level molecular view of an innate host defense lectin inhibiting its viral glycoprotein target.

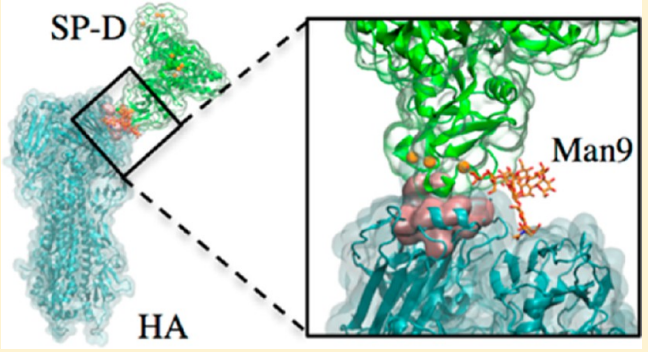

Influenza A virus (IAV) poses a major global biothreat to humans and animals. Newly emerging viral strains and viruses from animal reservoirs are responsible for IAV outbreaks that cause widespread illness before vaccines can be developed. Initial host defense is provided by the innate immune system, which can neutralize novel viral strains without prior recognition. One of the host's innate strategies against influenza relies on collagenous lectins (collectins), which are present in respiratory lining fluids where they participate in front-line defense against pathogens. Pulmonary collectins, including surfactant protein D (SP-D), are calcium-dependent (C-type) mammalian lectins that are involved in a wide range of immune functions.[1−4] SP-D, a pattern recognition receptor present in mucosal secretions, targets glycoproteins on viruses, bacteria, fungi, yeast, and allergens.[5,6] SP-D mediates a wide range of anti-influenza activities,[7−12] including inhibition of hemagglutination, viral aggregation, and neutralization. The major IAV target for SP-D is the viral glycoprotein hemagglutinin (HA), a major virulence factor that packs densely on the viral surface. HA plays a central role in influenza infection. It is responsible, through its sialic acid receptor site, for attaching IAV to sialylated glycoproteins on host cells and facilitating entry of the viral genome. HA on its own surface expresses high-mannose glycans, particularly a highly branched nonamannose (Man9), which are recognized by SP-D through lectin activity. There is accumulating evidence that increased

Received: August 6, 2013
Revised: October 25, 2013
Published: November 13, 2013

virulence of HA strains is correlated with evasion of SP-D innate surveillance through loss of HA glycosylation.[8,9,13,14]

Collectins are secreted multidomain C-type (calcium-dependent) lectins with a short N-terminal domain, a collagen-like domain, an α-helical neck domain, and a carbohydrate recognition domain (CRD), which contains the lectin site. Recombinant production of the neck and carbohydrate recognition domain (NCRD) yields a trimeric unit with lectin activity, capable of binding saccharides and pathogens. Interestingly, whereas wild-type human SP-D NCRD (WT) binds saccharides and HA but exhibits poor antiviral activity,[15−17] gain-of-function NCRD mutants can be engineered to perform such activities at levels approaching or exceeding those of native collectins.[16] These mutants are able to aggregate IAV particles, which is surprising given that they lack the N-terminal and collagen domains of SP-D that are associated with oligomeric assembly, increased avidity, and the neutralizing and aggregating activity of native SP-D.[16] This attribute of these mutants was unexpected and up to now unexplained. The mutants have provided a valuable probe into correlations between HA interactions and antiviral activity *in vitro* and *in vivo*. For example, we have reported that unlike WT, D325A+R343V inhibits seasonal and poorly glycosylated pandemic strains of IAV and protects against influenza infection upon being administered intratracheally to mice.[16]

Molecular recognition between viral glycoproteins and lectins involved in the innate immune response is poorly understood; little is known beyond the basic knowledge that carbohydrate targets are involved. Although dozens of crystal structures of HA and of several complexes with antibody Fab fragments have been reported,[18−21] no protein−HA complexes with innate host defense proteins have been studied at the atomic level. Previous computational studies of lectins with anti-influenza activity, namely of SP-D,[22,23] mannan-binding lectin,[24] and galectins,[25,26] have focused on complexes with isolated carbohydrate ligands rather than with viral glycoproteins. Similarly, computational studies of hemagglutinins[27−29] have not addressed binding to lectins; a major barrier has been the large size of the system, necessitating advanced computational approaches.

In this study, we have used X-ray crystallography, molecular modeling, and large-scale molecular dynamics to probe the interactions between SP-D and HA at the atomic level. Our studies target HA from the A/Aichi/68/H3N2 strain of IAV (also known as X31). This HA has only one N-linked glycan on the head domain, at residue 165, an important glycosylation site location for H3N2 strains,[7] as a lack of this residue is associated with collectin resistance.[9] We demonstrate that native SP-D possesses antiviral activity against the Aichi strain, indicating that the 165 *N*-glycan is sufficient for SP-D recognition of IAV. We have shown previously that SP-D does not inhibit PR-8 (A/Puerto Rico/8/1934/H1N1), an IAV strain that has no HA head glycans, and that SP-D strongly inhibits Phil82 (A/Philippines/1982/H3N2), which has a sequence that is >90% identical with that of Aichi and contains the 165 N-linked glycan among other head glycans.[9] This study offers the first computational investigation involving a complex of a full hemagglutinin trimer and a trimeric NCRD of SP-D. Additionally, the binding affinity between the HA glycan and SP-D has been studied and compared with experimental data. Comparisons between WT and D325A+R343V SP-D NCRDs allow the linking of viral neutralization to molecular properties underlying HA−SP-D binding, thereby promoting an improved understanding of the recognition of IAV by innate host defense molecules.

EXPERIMENTAL PROCEDURES

Preparation of Materials. Recombinant human SP-D NCRD was prepared as described previously[30,31] with an N-terminal S tag for the neutralization assays, or as a tagless molecule with an additional truncation of seven residues at the amino terminus of the neck region to facilitate crystallization.[30] The Aichi (A/Aichi/68/H3N2) strain was obtained from American Type Culture Collection, propagated in hens' eggs, and purified as described previously.[8] The synthetic non-amannoside (Man9) with a methyl group rather than Asn at the reducing end was prepared as described previously,[32] and the analytical data are in agreement with previous reports.[33]

Fluorescent Focus Assay of IAV Infectivity. MDCK cell monolayers were prepared in 96-well plates and grown to confluency. These layers were then infected with diluted IAV preparations for 45 min at 37 °C in PBS with 2 mM calcium and magnesium. After being incubated for 45 min, the cells were washed with MEM containing 10% FBS and 1% P/S. They were then incubated for an additional 6.25 h in this medium. MDCK cells were then tested for the presence of IAV-infected cells using a monoclonal antibody directed against the influenza A viral nucleoprotein (provided by N. Cox, Centers for Disease Control and Prevention, Atlanta, GA) as previously described.[22] IAV was preincubated for 30 min at 37 °C with various concentrations of collectins or control buffer, followed by addition of these viral samples to the MDCK cells. Similar assays were also performed using undifferentiated primary human tracheo-bronchial epithelial cells obtained from ATCC and cultured following the manufacturer's recommendations.

Crystal Structure Determination. Crystals of D325A+R343V were grown in hanging drops by mixing equal amounts of purified D325A+R343V [12−15 mg/mL in 20 mM HEPES buffer (pH 7.5), 150 mM NaCl, and 10 mM calcium acetate] and the reservoir solution [0.1 M HEPES buffer (pH 7.5), 0.25 M NaCl, and 20−22% (w/v) PEG 3350] on a siliconized coverslip and equilibrating over a sealed well containing 0.5 mL of the reservoir solution at 17 °C. Large crystals grew within a few days. For ligand soaking, crystals were transferred to the reservoir solution in which solid Man9 was dissolved at a concentration of 0.5 or 10 mM. Crystals were soaked for 2 h (0.5 mM Man9) or overnight (10 mM). Prior to freezing in a cold nitrogen stream, the crystals were soaked in the Man9 solution with either 1 M 1,6-hexanediol (0.5 mM Man9) or 15% (v/v) ethylene glycol (10 mM) for ∼20 s as a cryoprotectant. X-ray diffraction data were collected on an RAXIS-IV image plate detector with an RU-300 rotating anode X-ray generator. Data integration, indexing, merging, and scaling were performed using DENZO and Scalepack.[34] The structure was determined by molecular replacement using the previously determined structure of R343V SP-D complexed with α-1,2-dimannose, less the waters and ligands and incorporating the expected D325A mutation as well as the truncation of the construct, as a search model using the AutoMR program in Phenix.[35] The determined structure contains four trimers. The low-resolution structure was determined by difference Fourier transformation using the high-resolution structure as a starting model. Iterative cycles of manual rebuilding and refinement were performed using Coot[36] and Phenix. In both cases, metal restraints were used throughout refinement as defined by ReadySet in Phenix. For

the low-resolution structure, noncrystallographic symmetry restraints on the protein torsion angles were used throughout. In the final steps of refinement for the liganded structure, TLS parameters were refined for both structures with two zones per monomer used, one for the neck (residues 214−232) and one for the CRD (residues 233−355).

Molecular Modeling. To create the starting model for molecular dynamics calculations, coordinates from three crystal structures were assembled to form an initial HA−Man9−SP-D complex. The model employed the HA crystal structure from the A/Aichi/68/H3N2 strain [Protein Data Bank (PDB) entry 1HGE].[37] This structure was selected because it has only one glycan on the HA head at N165. The first three sugars of this N-linked glycan (residues Nag500, Nag501, Bma502 in Figure 1) are visible in the crystal structure, and the remainder of the

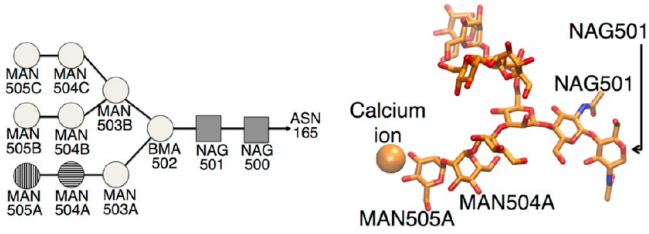

Figure 1. Schematic diagram (left) and structure (right) of the Man9 glycan of HA. In the left panel, mannose (Man) residues are represented as circles and *N*-acetylglucosamine (Nag) residues as squares. Man504 and Man505 interact with calcium ions in D325A +R343V and WT and are differentiated to specify in the text which sugar residue actually directly contacts the ions. Nag residues connect Man9 to Asn165 of HA. In the right panel, Man505A (conformation used in this work) binds to the lectin calcium ion of WT, shown as an orange sphere. Man9 and Nag are represented as licorice with oxygens colored red, carbons orange, nitrogens blue, and hydrogens white.

complex was built onto this glycan. To attach the SP-D trimer, the mannose chain present in the D325A+R343V crystal structure (comprising Man505A, Man504A, and Man503A) was extended by one mannose (equivalent to residue Bma502) using the computational tools in Maestro (Schrödinger, LLC, New York, NY). This added mannose was then superimposed onto the Bma502 residue from chain A of the HA crystal structure. Removal of the added mannose from the SP-D model resulted in a HA−Man4−SP-D complex. To complete the five remaining mannoses, the Bma502 residue of the visible Man8 chain from an Fab−Man9 crystallographic complex (PDB entry 3TV3[38]) was superimposed onto Bma502 of the HA model, and Man503B, Man504B, Man504C, and Man505C from the superimposed coordinates were added to the model. To complete the HA−Man9−SP-D model, Man505B was added with Maestro. The glycosidic bonds of sugars added in Maestro were set to initial torsion angles of −60° and 0° for φ and ψ, respectively, values that are in the favored region of the conformational energy map for the dimannose linkages created[39] and introduce no major steric clashes with other atoms in the model. Figure 1 shows the resulting model of the Man9 component of the D325A+R343V−HA complex. This model was the only one consistent with the crystallographic data and favorable glycosidic linkages.

Because the objective of the molecular dynamics (MD) simulations is to compare the WT−HA and D325A+R343V−HA complexes, the starting coordinates of both models need to be chosen to be as similar as possible. In wild-type or mutant SP-D crystal structures, residues at positions 325 and 343 do not interact in any way, nor is there any evidence that the side chains contribute to the overall conformation of the lectin site.[15,16,40] Therefore, we used the coordinates of the D325A +R343V−HA complex as a template to obtain the starting model for WT. We restored the WT structure by mutating Ala325 and Val343 back to Asp325 and Arg343, respectively. These mutations were made using VMD.[41] Additionally, the Man9 chain had to be remodeled because WT binds to the reducing end of the mannose 9 (Man9) chain (circle with vertical stripes), while D325A+R343V binds to the non-reducing end (circle with horizontal stripes) as shown in the schematic diagram in Figure 1.

To model the Man9 chain in the WT−HA complex, two mannose residues (Man504A and Man505A), which interact with the lectin site of SP-D, were replaced by two corresponding mannose residues found in the WT−dimannose complex (PDB entry 3G83[15]). The latter two residues were manually connected to the seven remaining mannose residues, resulting in a long bond connecting Man503A and Man504A. To correct this long bond, energy minimization was performed for 10000 steps on the Man9 chain while restraining the coordinates of Man504A, Man505A, and the protein complex. All mannose residues in the minimized complex were found in our calculations to be in the stable chair conformation, indicating that the rearrangement of the Man9 chain did not introduce large steric and torsional strains into the chain.

Molecular Dynamics (MD) Simulations. Figure 2 shows the protein system that was simulated for this study: the HA

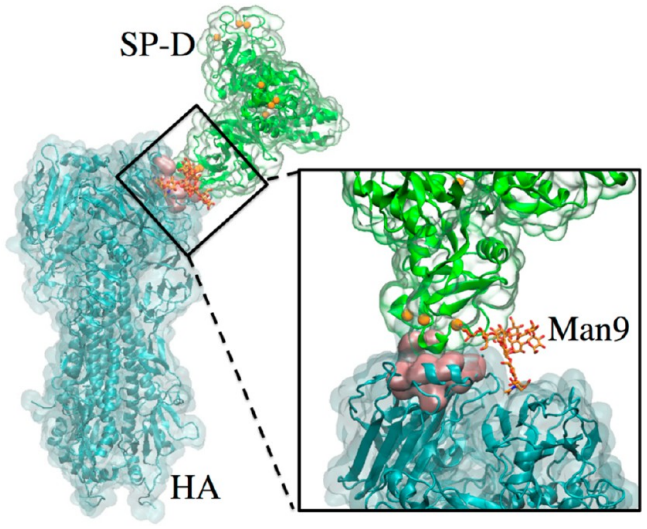

Figure 2. View of the entire simulated system. Hemagglutinin (HA) is shown as a cartoon and transparent surface representation (cyan), and lung surfactant protein-D (SP-D) is shown as a cartoon and transparent surface representation (green). HA and SP-D are connected noncovalently through a Man9 chain, shown enlarged in the inset with the sialic acid binding site shown with a pink surface representation, and the calcium ions of SP-D are shown as orange spheres. Water molecules and ions are not shown.

trimer glycosylated with one Man9 and complexed with one trimer of SP-D (either WT or D325A+R343V) with bound calcium ions. Table 1 lists sizes and time scales of the simulations conducted in this study. Each complex was solvated in a sufficiently large water box that the minimal distance between the complex and the boundary of the water box is 15 Å

dx.doi.org/10.1021/bi4010683 | *Biochemistry* 2013, 52, 8527−8538

Table 1. Simulations Performed in This Study

simulation	description	time (ns)	no. of runs
WTS	wild type, equilibration of the WT−HA complex with the Man9 chain	100	3
DMS	double mutant, equilibration of the D325A +R343V−HA complex with the Man9 chain	100	3
WTNS	wild type without sugar, equilibration of the WT−HA complex without the Man9 chain	100	1
DMNS	double mutant without sugar, equilibration of the D325A+R343V−HA complex without the Man9 chain	100	1
SMS	single mutant, equilibration of the R343V−HA complex with the Man9 chain	100	1
DMNC	double mutant without calcium, equilibration of the D325A+R343V−HA complex with the Man9 chain and without calcium ions	7	1

along all three axes. The system was neutralized with 150 mM NaCl to match the optimal salt concentration present in *in vitro* experiments.[42] The final simulated systems contain approximately 320000 atoms, including proteins, water molecules, and ions.

The systems described were subjected to conjugate gradient minimization for 50000 steps and subsequently heated to 310 K in <4 ps. The procedure was followed by a 0.5 ns equilibration with all protein and sugar atoms fixed under an *NPT* ensemble, and a 2 ns equilibration under an *NVT* ensemble. Finally, 100 ns production simulations under an *NVT* ensemble were performed. To ensure that the starting structures retain the key interactions, the hydrogen bond network and other noncovalent interactions between O3 and O4 of the calcium-bound mannose residue and the SP-D protein were maintained by imposing virtual springs to constrain their distances. The constants of these virtual springs were set to 50 kcal mol^{-1} Å^{-2} during minimization, 20 kcal mol^{-1} Å^{-2} during *NPT* ensemble equilibration, and 10 kcal mol^{-1} Å^{-2} during *NVT* ensemble equilibration. The constraints were removed in the final 100 ns simulation.

All coordinated ligands of the calcium ion were restrained to circumvent potential force field limitations and preserve the bidentate property of calcium-bound mannose (see the Supporting Information). All eight coordinated ligands were constrained with a harmonic potential of the form $U(x) = k(x - x_{ref})^2$, where k was 1000 kcal mol^{-1} Å^{-2} and x_{ref} was set to 2.41 Å[43] throughout minimization, heating, equilibration, and final 100 ns simulations. The constraint is a reasonable approach given the submicrosecond time scale of our simulations; unbinding rates of calcium-bound ligands are measured experimentally to be on the order of seconds to minutes[44] such that unbinding, impossible with the constraints imposed, is expected to be very rare.

Simulations were performed using NAMD version 2.9[45] assuming the CHARMM27 force field with CMAP corrections[46] for the protein and assuming the TIP3P model for water molecules.[47] The CHARMM36 force field was used for the sugars.[48,49] Periodic boundary conditions were assumed, and the particle mesh Ewald summation method was employed for the evaluation of Coulomb forces. The van der Waals energy was calculated using a cutoff of 12 Å. The temperature and pressure were maintained at 310 K and 1 atm, respectively, using a Langevin thermostat with a damping constant of 1 ps^{-1} and Nosé-Hoover Langevin piston methods.[50] The integration time step was 1 fs.

Residue-based interaction energies between SP-D and HA were calculated using a modified generalized Born (GB) model.[51] This model considers van der Waals interaction, electrostatics, and a solvation energy component that takes solvent polarization into account. The solvent model did not include hydrophobic interactions, unlike the GB−molecular surface area approach.[52] However, the GB model is a sufficiently good approach for quantifying the interaction energies because the interactions between SP-D with HA and Man9 involve mostly polar residues.

RESULTS

Fluorescent Focus Assay. We used a fluorescent focus assay for viral neutralization to compare the ability of full-length SP-D and SP-A and the various NCRD preparations to inhibit the infectivity of the H3N2 pandemic IAV strain Aichi68 *in vitro*. We previously reported that D325A+R343V had neutralizing activity equivalent to that of native SP-D for a seasonal H3N2 strain.[16] As shown in Figure 3A, D325A

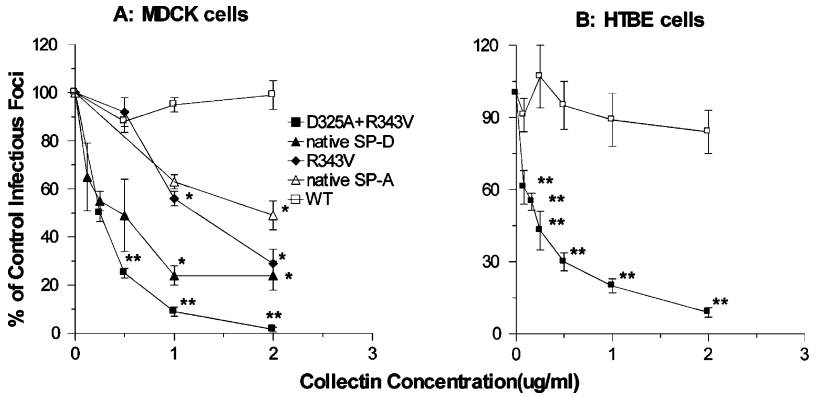

Figure 3. Viral neutralizing activity of SP-D NCRDs (WT NCRD, R343V, and D325A+R343V) and native SP-D and SP-A against Aichi68 H3N2. Aliquots of the Aichi68 viral strain were incubated with the indicated concentrations of various native collectin or NCRD preparations. The samples were then used to infect MDCK cell monolayers (A) or HBTE cells (B) and tested for infectious foci 7 h later using anti-nucleoprotein antibodies and fluorescence detection. WT did not inhibit Aichi68 in either cell type. R343V or native SP-D and SP-A were inhibitory (one asterisk indicates $p < 0.05$ vs control). D325A+R343V caused significantly greater inhibition than any of the other NCRDs tested (two asterisks indicate $p < 0.02$ compared with other NCRDs and control). The results are means ± the standard error of the mean of three (A) or four (B) experiments.

dx.doi.org/10.1021/bi4010683 | *Biochemistry* 2013, 52, 8527−8538

Table 2. Crystallographic Data Collection and Refinement Statistics

	unliganded D325A+R343V	Man9−D325A+R343V complex
	Data Collection	
space group	$P2_12_12_1$	$P2_12_12_1$
unit cell dimensions	a = 107.524 Å, b = 160.108 Å, c = 160.073 Å, $\alpha = \beta = \gamma = 90°$	a = 107.833 Å, b = 159.454 Å, c = 159.894 Å, $\alpha = \beta = \gamma = 90°$
resolution (Å)	15−2.1 (2.17−2.10)	15−3.2 (3.3−3.2)
no. of unique reflections	154671 (12482)	45301 (4406)
completeness (%)	95.8 (78.3)	99.6 (98.1)
mosaicity (deg)	0.653	0.778
redundancy	5.8 (4.2)	4.2 (3.5)
$I/\sigma I$	13.9 (4.8)	8.2 (2.8)
data cutoff	$I > -3\sigma$	$I > -3\sigma$
R_{merge}	0.073 (0.324)	0.169 (0.431)
	Refinement	
R_{work}/R_{free}	0.1627/0.1878	0.1868/0.2222
no. of reflections	154598	45242
twin fraction (operator)	0.490 ($-h,l,k$)	0 (none)
total no. of atoms	14057	13487
no. of protein atoms	12789	13049
no. of calciums and ligands	36	424
no. of waters	1232	14
mean B value (Å^2)	29.9	49.2
protein atoms	29.9	48.7
calcium and ligands	34.5	67.1
waters	30.0	20.2
deviations from ideal		
bond lengths (Å)	0.011	0.014
bond angles (deg)	0.572	0.753
Ramachandran plot (%)		
favored	97.11	97.82
allowed	2.59	2.18
outliers	0	0

+R343V strongly inhibited the Aichi68 strain in MDCK cells. The strong activity of D325A+R343V was confirmed in primary HTBE cells, as well (Figure 3B). The WT had no inhibitory activity in either assay. We note that D325A+R343V also had stronger neutralizing activity than either R343V or native SP-D or SP-A. The 50% neutralizing concentration for D325A +R343V was ∼0.25 μg/mL, whereas the corresponding concentration for native SP-D, the next best inhibitor, was ∼0.50 μg/mL.

D325A+R343V Crystal Structures. The crystal structure of unliganded D325A+R343V was determined at 2.1 Å resolution and in complex with Man9 at 3.2 Å resolution. The final structures show good geometry and agreement with the diffraction data (Table 2). The D325A+R343V crystals are in a different space group than R343V or WT[15] and have more monomers in the asymmetric unit (12 vs 3). In the D325A +R343V complex, only three mannose sugars are visible in the electron density map, all linked with α1−2 glycosidic bonds, and therefore, these sugars have been assigned as Man505A, Man504A, and Man503A of Man9 based on the connectivity. The third sugar (Man503A) is less well-defined in the electron density maps (and absent in two of the monomers in the asymmetric unit) and occupies space made available by the Asp325 to Ala mutation. Ligands are oriented similarly in all 12 subunits.

The unliganded and complexed D325A+R343V structures are similar, with a root-mean-square deviation (rmsd) of 0.2−0.6 Å. The protein portion of the D325A+R343V complex is structurally similar to those of the WT and R343V single-mutant dimannose complexes.[15] The superimposed monomers have rmsd values of 0.4−0.7 Å, calculated using all protein α-carbons in the NCRD for the two available structures (PDB entries 3G83 and 3G84).

In the D325A+R343V complex with Man9, the ligand is bound in a conformation and location similar to those of the α1,2-dimannose complex with R343V. In D325A+R343V, as for R343V, one sugar (Man504A) is bound in the lectin site, making coordination interactions to the calcium ion through the 3- and 4-hydroxyl groups of the mannose sugar. The nonreducing end sugar (Man505A) is bound above Val343. Overall, the Asp325 to Ala mutation shows little effect on the binding of dimannose: the sugars have rmsd values between 0.4 and 1.0 Å calculated using all non-hydrogen dimannose atoms in the superimposed single- and double-mutant protein structures.

MD Simulations. In simulations WTS and DMS (Table 1), both WT and D325A+R343V are found to be stably bound to HA. Furthermore, both SP-D proteins are seen to block the sialic acid binding site of HA (Figure 4). To quantify the inhibition of the sialic acid binding site by SP-D, the sialic acid (SA) accessible surface area (ASA) was calculated using the rolling ball algorithm.[53] Instead of using the radius of a water molecule, i.e., 1.4 Å for the rolling probe, we used the radius of gyration of sialic acid, i.e., 3.0 Å, to evaluate the ASA. As shown in Figure 5, both WT and D325A+R343V resulted in similar SA ASA values of approximately 150 Å^2 at the end of either simulation, conducting in each case an average over three independent trajectories. At the beginning of the simulation,

dx.doi.org/10.1021/bi4010683 | Biochemistry 2013, 52, 8527−8538

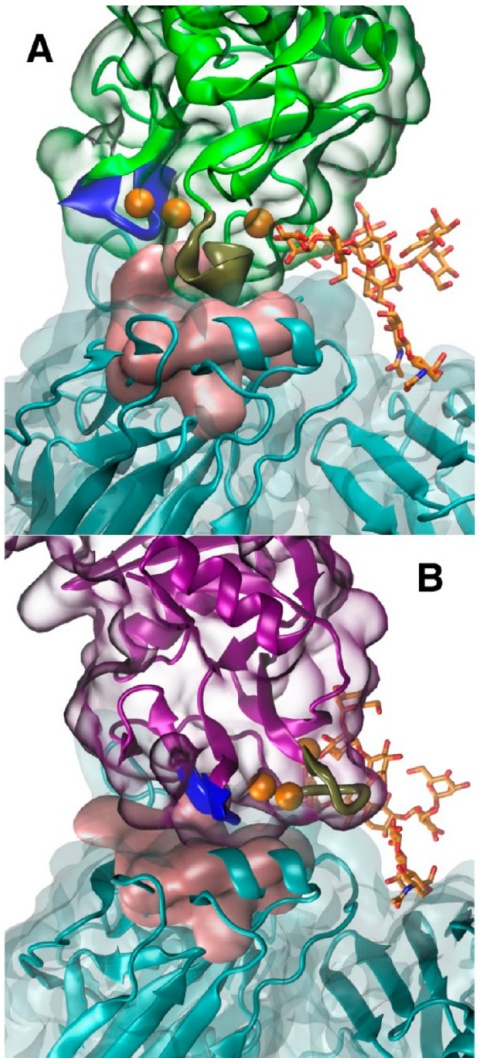

Figure 4. Inhibition of the sialic acid binding site. The binding site, located on HA, is shown as a pink surface. The remainder of HA is shown as a cartoon and transparent surface representation (cyan). The Man9 chain linked to HA is shown as red-orange licorice. (A) HA bound to WT, the latter shown as a cartoon and transparent surface representation (green). (B) HA bound to D325A+R343V, the latter shown as a cartoon and transparent surface representation (purple). Two loop regions of both WT and D325A+R343V, colored tan and blue, are seen to cover and thereby inhibit the sialic acid binding site.

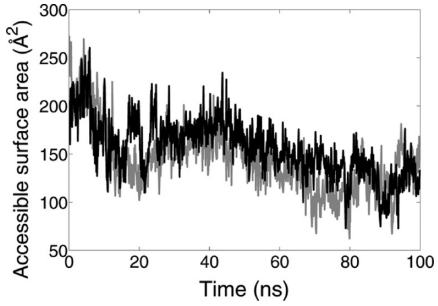

Figure 5. Accessible surface area of the HA sialic acid binding site. Shown is the time evolution of the average sialic acid binding site accessible surface area for WT (black) and D325A+R343V (gray) bound to HA.

the SA binding site was only partially blocked by SP-D as reflected in an SA ASA value of 200 Å^2. The decrease in SA ASA over time implies that the SA binding site becomes less accessible to SA during the course of the simulation. Given that the SA ASA for a fully exposed SA binding site is approximately 450 Å^2, it is apparent that both WT and D325A+R343V SP-D fully block the SA binding site at the end of the simulations.

The energies of interaction between SP-D and HA residues were also monitored. The average total energies of interaction between SP-D with HA and the Man9 chain are −123 ± 8 and −142 ± 14 kcal/mol for WT and D325A+R343V, respectively; the energies of interaction between SP-D and the Man9 chain alone are −87 ± 7 and −97 ± 5 kcal/mol for WT and D325A +R343V, respectively. Table 3 shows that the mannose residue,

Table 3. Average Interaction Energies of Residues between SP-D and the Man9 Chain Only in Simulations WTS and DMS[a]

residue (WT/D325A +R343V)	average energy for WT (kcal/mol)	average energy for D325A+R343V (kcal/mol)	difference (kcal/mol)
Man503A	−1.9 ± 1.4	−5.1 ± 0.7	3.2 ± 2.0
Man505A/Man504A*	−69.0 ± 0.5	−69.6 ± 0.4	0.5 ± 0.9
Man504A/Man505A	−11.2 ± 5.1	−14.8 ± 1.8	3.7 ± 6.9
remaining residues in the Man9 chain	−4.9 ± 1.9	−7.7 ± 5.5	2.8 ± 7.4

[a]The three mannose residues closest to the calcium ion interact strongly with SP-D. The mannose residue that directly interacts with the calcium ion of the SP-D is labeled with an asterisk.

which is directly bound to the SP-D lectin calcium ion, accounts for approximately half of the total interaction energy of the protein complex. Such a significant contribution to this interaction underscores that the sugar−calcium ion interaction at the lectin site is essential for the binding of SP-D to saccharide ligands.

Two key loop regions were seen in the simulations to inhibit the sialic acid binding site of HA. Table 4 lists interaction energies for different residues of SP-D. Residues 300−304 in the short loop (residues 297−304) show lower interaction energies for D325A+R343V, while residues 324−329 in the long loop (residues 307−331) indicate lower energies for WT. Residues 300−304 of D325A+R343V are observed to inhibit the SA binding site, while residues 324−329 of WT inhibit this site. Residues 300−304 and 324−329 are colored blue and tan, respectively, in Figure 4.

In the simulations, the binding of HA with D325A+R343V, but not with WT, reveals the involvement of hydrophobic interactions. Figure 6A illustrates the difference in average hydrophobic interaction between SP-D and HA for WT and D325A+R343V. As shown in Figure 6B, Ala325 of D325A +R343V is observed to interact with another hydrophobic residue of HA, Trp222. Additionally, Pro319 of D325A+R343V interacts with Ala138 of HA throughout the entire trajectory. It is evident that the Asp-to-Ala mutation of residue 325 increases the strength of the hydrophobic interaction between D325A +R343V and HA and provides additional stabilization to the complex. This hydrophobic interaction may provide a basis for the enhanced HA binding by the D325A+R343V mutant compared with the HA binding by the R343V mutant.

As shown in Figure 7, charged residues Arg343 and Asp325 in WT stabilize Man9 chain binding through the formation of hydrogen bonds. As a result of the two mutations, the Man9

dx.doi.org/10.1021/bi4010683 | *Biochemistry* 2013, 52, 8527−8538

Table 4. Average Interaction Energies of Residues between SP-D and HA and the Man9 Chain in Simulations WTS and DMS[a]

residue (WT/D325A+R343V)	average energy for WT (kcal/mol)	average energy for D325A+R343V (kcal/mol)	difference (kcal/mol)	label
Thr300	−1.2 ± 0.3	−2.9 ± 2.1	1.7 ± 2.4	
Glu301	−5.1 ± 1.8	−6.8 ± 4.0	1.7 ± 5.8	
Gly302	−1.6 ± 1.2	−4.0 ± 0.7	2.7 ± 1.9	
Lys303	−1.6 ± 1.1	−3.8 ± 0.2	2.2 ± 1.3	
Phe304	−0.3 ± 0.1	−1.8 ± 1.1	1.5 ± 1.2	
residues 300−304	−9.8 ± 4.0	−19.3 ± 5.1	9.5 ± 9.1	short loop
Asp324	−4.5 ± 3.4	−2.4 ± 1.2	−2.0 ± 4.6	
Asp325/Ala325	−9.4 ± 2.5	−4.2 ± 0.3	−5.2 ± 2.8	
Gly326	−4.1 ± 0.8	−1.5 ± 0.1	−2.6 ± 0.9	
Gly327	−4.2 ± 2.1	−0.5 ± 0.1	−3.7 ± 2.2	
Ser328	−1.6 ± 0.8	−0.3 ± 0.0	−1.3 ± 0.8	
Glu329	−12.4 ± 0.9	−7.6 ± 0.2	−4.8 ± 1.1	
residues 324−329	−36.1 ± 4.8	−16.5 ± 1.5	−19.6 ± 6.3	long loop
Glu333	0.4 ± 1.3	−14.6 ± 0.4	15.0 ± 1.7	
Arg343/Val343	−10.7 ± 4.5	−0.8 ± 0.1	−9.9 ± 4.6	

[a]Positive values in the difference column indicate that the corresponding residues of D325A+R343V contribute more to the overall stability than they do for WT. The interaction energies are averages over three independent simulations.

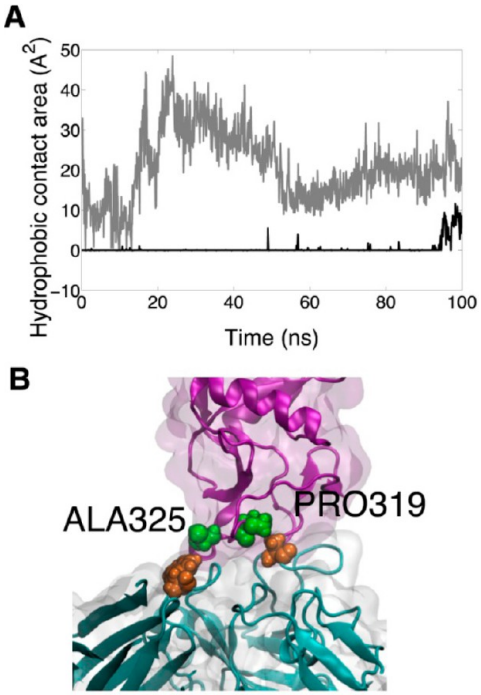

Figure 6. Hydrophobic interaction formed between SP-D and HA. (A) Shown is the time evolution of the average hydrophobic contact area between HA and WT (black) or D325A+R343V (gray) in simulations WTS and DMS. (B) HA and D325A+R343V are shown as a cartoon and transparent surface representation (cyan and purple, respectively). Hydrophobic interactions arise mainly between Ala325 and Pro319 of D325A+R343V (green) and Trp222 and Ala138 of HA (dark orange).

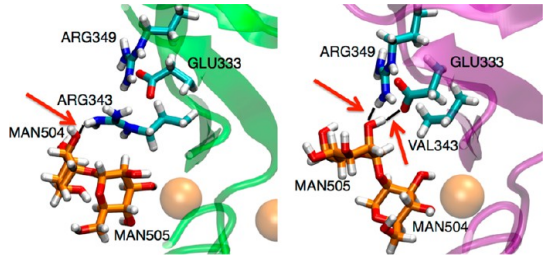

Figure 7. R343V mutation alters the Man9 binding mode. Shown is the difference in hydrogen bond networks for the Man9 chain binding to WT (left) and D325A+R343V (right). The red arrows point to the hydrogen bonds, which are represented as black solid lines. WT and D325A+R343V are shown as green and purple transparent cartoon representations, respectively. D325A+R343V calcium ions are shown as orange spheres. Mannose residues are shown as licorice with oxygens colored red, carbons orange, and hydrogens white. Protein residues are shown as licorice with oxygens colored red, carbons cyan, nitrogens blue, and hydrogens white.

chain becomes engaged in a strong hydrogen bond formed between Glu333 and Man505A (Table 5).

Despite the stability of the SP-D−HA complexes in the presence of Man9, SP-D is seen to diffuse away from the SA binding site within the first 40 ns in the absence of the glycan as shown in Figure 8, though D325A+R343V without glycan is observed to diffuse back to its starting location. These results justify the time scale of the simulations; i.e., if an SP-D−HA complex is not stably bound together, the SP-D has sufficient time in our simulations to leave the SA binding site by diffusion.

The 7 ns DMNC simulation showed that SP-D with its calcium ions removed became dissociated from the Man9 chain in 7 ns (see the Supporting Information), illustrating the importance of the calcium ion for the function of SP-D.

DISCUSSION

We have undertaken a crystallographically informed molecular dynamics approach to investigating the interaction of SP-D with HA glycans and its influence on antiviral activity. Nuclear magnetic resonance and molecular dynamics approaches,[54,55] together with statistical analyses,[56−58] show that despite the inherent flexibility of glycosidic linkages, branched high-mannose glycans such as those found on viral surfaces have a limited number of overall conformations. These structures can be recognized by pattern recognition receptors such as C-type lectins of the innate immune system. Binding of mannosyl

dx.doi.org/10.1021/bi4010683 | Biochemistry 2013, 52, 8527−8538

Table 5. Occupancy Percentages of Hydrogen Bonds between SP-D and the Man9 Chain during Simulations WTS and DMS[a]

WT−Man9 chain			D325A+R343V−Man9 chain		
donor	acceptor	occupancy (%)	donor	acceptor	occupancy (%)
Man505A	Glu329	100	Man504A	Glu329	100
Man505A	Glu321	100	Man504A	Glu321	100
Asn341	Man505A	88	Asn341	Man504A	92
Asn323	Man505A	86	Asn323	Man504A	52
Arg343	Man504A	24	Val343	Man505A	0
Man505A	Asp325	54	Man504A	Ala325	0
Man504A	Glu333	0	Man505A	Glu333	100
Arg349	Man504A	0	Arg349	Man505A	14

[a]During these simulations, a strong hydrogen bond is formed between Glu333 and the extended mannose. The first four rows are for the main hydrogen bonds that stabilize the binding of the Man9 chain at the lectin site. The last four rows highlight the difference in glycan binding between WT and D325A+R343V. All hydrogen bonds among polar atoms (N, O, S, and F) are selected with a cutoff distance of 3.5 Å and an angle tolerance of 50°.

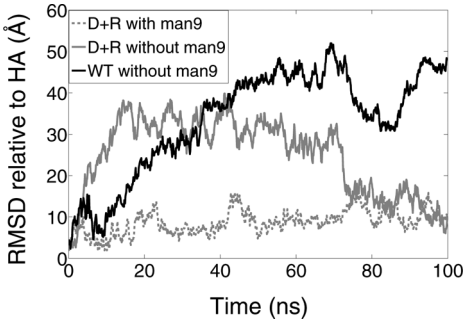

Figure 8. Role of the Man9 chain in stabilizing the complex between SP-D and HA. A comparison of simulations DMS, DMNS, and WTNS demonstrates the role of the sugar in stabilizing the complex between SP-D and HA. Shown is the time evolution of the rmsd of SP-D relative to HA for WT (black) and D325A+R343V (gray) without the Man9 chain and for D325A+R343V with the Man9 chain.

oligosaccharides has been explored structurally for several C-type lectins, including SP-D,[15,40] mannose binding protein,[59−63] dendritic cell surface receptor DC-SIGN, and endothelial cell receptor DC-SIGNR,[64−68] all of which recognize N-linked glycans on viral pathogens such as influenza and HIV. The crystallographic complexes are similar overall in that the major point of contact between sugar and protein is at the lectin site; significant contacts with other lectin residues are sparse. Nonetheless, nearby residues, e.g., Asp325 and Arg343 in SP-D,[15,40] influence spatial accessibility for portions of the branched oligosaccharide chains, thereby imposing a degree of selectivity. Our previous studies of SP-D have shown that mutating these residues greatly influences antiviral activities, with D325A+R343V gaining significant functional capabilities compared with WT. Therefore, our studies focus on the dynamic properties of both WT and mutant SP-D with respect to *N*-glycan binding and HA inhibition.

Our computational studies of binding of SP-D to Aichi HA show excellent agreement with experimental data for binding of SP-D to HA from Phil82, another H3N2 strain containing glycan 165. The critical importance of the lectin activity in the interaction is underscored in two sets of simulations, WTNS and DMNS, in which both WT−HA and D325A+R343V−HA complexes exhibit significant fluctuation and drifting in 100 ns when the Man9 chain is absent (Figure 8). Similar results were obtained in simulations with porcine SP-D.[22] In prior SPR experiments with Phil82 HA, D325A+R343V was found to bind more tightly than WT, with mean apparent K_d values of 0.04 and 0.231 nM for D325A+R343V and WT, respectively.[16] The computational results with Aichi HA are consistent with the experimental Phil82 HA data in that while WT and D325A +R343V both bind to the viral glycoprotein, D325A+R343V binds with a higher affinity (Table 4). The computational results further suggest that the stronger HA binding by D325A +R343V may be due, in part, to higher glycan binding affinity. Table 3 shows that compared with WT, D325A+R343V binds more strongly to the Man9 chain by approximately 10 kcal/mol. These results are consistent with carbohydrate microarray experiments in which R343V, which shares the same arginine mutation as D325A+R343V, binds more strongly to branched mannose oligosaccharides than does WT.[15]

The nature of the mutations appears to play a role in the differences between WT and D325A+R343V in binding Man9. Table 3 shows a difference in interaction energies for two neighboring mannose residues, namely, Man505A and Man503A for D325A+R343V and Man504A and Man503A for WT. These data suggest that an increase in interaction energy at Man505A is due to the Arg343 to Val mutation, consistent with structural evidence.[15] Detailed hydrogen bond searching allows determination of the key residue that interacts most strongly with the extended glycan chain. The formation of hydrogen bonds between Glu333/Arg349 and Man505 (labeled in Figure 7) is potentiated by the Arg343 to Val mutation, which removes the steric hindrance caused by Arg343. Molecular dynamics simulations are able to reproduce this feature and suggest that a hydrogen bond between Man505 and Glu333 is more likely to form than between Man505 and Arg349. A decrease in interaction energy at Man503A suggests that the Asp325 to Ala mutation stabilizes the binding of the Man9 chain on SP-D. Ala325 is in the proximity of Man503A, suggesting loss of a steric constraint due to the Asp325 to Ala mutation. However, simulation SMS with the R343V single mutant does not support this hypothesis as it shows that Asp325 interacts strongly with Man503A because of the formation of hydrogen bonds. Further, crystallographic data regarding the role of Asp325 are obscured by this residue's involvement in crystal contacts.[40] Therefore, the underlying molecular mechanism of the effect of the Asp325 to Ala mutation on Man9 binding remains unclear.

Mannose interactions are not the only component of binding of D325A+R343V to HA. From the interaction energies calculated from simulations WTS and DMS, D325A+R343V binds more strongly than WT to HA by approximately 19 kcal/mol. After the subtraction of the interactions between SP-D and

dx.doi.org/10.1021/bi4010683 | *Biochemistry* 2013, 52, 8527−8538

the Man9 chain, it is observed that D325A+R343V still interacts more strongly with HA by an average of 9 kcal/mol. This difference may be explained by protein−protein interactions, particularly hydrogen bonds that form between the short and long loops of SP-D and the HA surface. It is important to note that the interaction energies do not account for hydrophobic contributions and that the D325A+R343V−HA complex has a higher interaction energy than the WT−HA complex if one takes only electrostatic interactions into account. As shown in Figure 5, D325A+R343V forms hydrophobic contacts with HA but WT does not. As a result, D325A+R343V binds more strongly to HA than does WT by more than 19 kcal/mol. The observation of hydrophobic interactions in the DMS simulation is novel in that protein−protein interactions in mammalian lectins have not been widely described.

The key loop interactions with the SA binding site of HA are different for WT and D325A+R343V. As seen in Figure 4, Table 4, and the interaction energies between SP-D and HA calculated for simulations WTS and DMS shown in Figure 5, residues 324−329 form the primary, long loop for WT that interacts with HA and inhibits its SA binding site. Interestingly, for pig SP-D, there is an insertion of three amino acid residues between residues 328 and 329.[69] The elongation increases the flexibility of the loop and may give rise to the enhanced inhibition of pig SP-D activity against IAV.[22,30,70] However, in contrast to WT and pig SP-D, the long loop of D325A+R343V contributes less to the overall stabilization of the complex; instead, in the D325A+R343V complex, short loop residues 300−304 interact primarily with HA at the SA binding site. Although the interaction energies for residues on the short loop fluctuate, the importance of the short loop for D325A+R343V could still be harnessed by averaging the energies over three independent trajectories.

In addition to using different loops, WT and D325A+R343V exhibit different modes of glycan binding that impact their interactions with the HA trimer. In crystallographic studies of α-1,2-dimannose complexes with WT or R343V, a reversed mode of dimannose binding is observed between the two proteins.[15] In WT, the nonreducing end of mannose (Man505A) is bound to the lectin site. In the mutant, Man505A occupies space vacated by the mutation and the reducing end mannose (Man504A) is bound in the lectin site, where it forms interactions similar to those of Man505A in the WT complex. Man504A in R343V is rotated 180° such that its O3 and O4 atoms are swapped compared to Man505A in WT (Figure 7). In this liganded D325A+R343V crystal structure, the double mutant binds to the dimannose moiety of Man9 in a manner similar to the binding of dimannose to R343V, providing further evidence that the Arg343 to Val mutation is responsible for the altered binding mode. Figure 9 shows how these different binding modes alter the overall orientation of the modeled HA−SP-D complexes.

We have proposed previously that in D325A+R343V, viral aggregation can be achieved by SP-D-mediated cross-linking of HA on neighboring viral particles. Experimental evidence from that study shows that trimeric D325A+R343V NCRD is nearly as effective at aggregating IAV as is native dodecameric SP-D, whereas the WT NCRD trimer does not aggregate or neutralize the virus.[16] These observations suggest that D325A+R343V is able to utilize a mechanism that circumvents the need for an extended oligomer to aggregate viral particles. Significant differences in the spatial orientation adopted by WT and D325A+R343V, such as those seen in Figure 9, could provide such a mechanism by altering the ability to cross-link HA and promoting viral aggregation and neutralization.

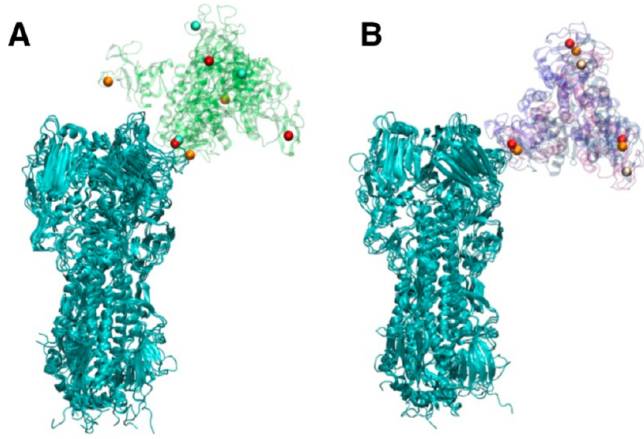

Figure 9. Differences in the orientation in HA complexes with WT (A) or D325A+R343V (B). The end points of three repeated simulations are overlapped for simulations WTS and DMS, respectively. Calcium ions are represented in van der Waals representation in orange, red, and white; WT and D325A+R343V are shown as green and purple transparent cartoon representations, respectively. HA is shown as a cyan cartoon representation.

In summary, simulation of entire SP-D−HA complexes has allowed us to investigate the detailed molecular interactions between SP-D and IAV HA. Using modeling and molecular dynamics approaches, we have determined that SP-D not only binds to the glycan chains on HA but also blocks the SA binding site upon binding to the glycan chains for the H3N2 strain that we studied. To test our hypotheses, site-directed mutants will be made in the short and long loops of SP-D to evaluate the *in vitro* and *in silico* properties of individual residues; e.g., systematic mutation of Ala325 to residues that vary in charge and size should alter interactions with Trp222 from HA. We also plan to investigate HA from other strains to test the generality of our conclusions. For example, HA glycan 104, a functionally important site found in most H1N1 strains, is also located near the SA site and may similarly block it. We additionally have suggested means through which binding of HA glycans by D325A+R343V could lead to an increased level of viral neutralization. On the basis of experimental and computational evidence, we speculate that the altered binding orientation and increased level of viral aggregation, perhaps coupled with the increased level of binding to HA by the mutant, enhance the ability of D325A+R343V to neutralize IAV. Viral aggregation studies of novel mutants should address this speculation. These studies thus shed light on how factors associated with HA binding correlate with antiviral activities of SP-D.

■ ASSOCIATED CONTENT

Supporting Information

Treatment of calcium ion coordination in the lectin site for molecular dynamics simulations and more details about simulation DMNC. This material is available free of charge via the Internet at http://pubs.acs.org.

Accession Codes

Atomic coordinates have been deposited as Protein Data Bank entries 4M17 and 4M18.

AUTHOR INFORMATION

Corresponding Authors

*(B.A.S.) Department of Physiology and Biophysics, Boston University School of Medicine, 715 Albany St., Boston, MA 02118. E-mail: seatonba@bu.edu. Telephone: (617) 638-5061. Fax: (617) 638-4041.

*(K.S.) Beckman Institute, University of Illinois, 405 N. Mathews Ave., Urbana, IL 61801. E-mail: kschulte@ks.uiuc.edu. Telephone: (217) 244-1604. Fax: (217) 244-6078.

Funding

Supported by National Science Foundation Grant PHY0822613 (K.S.), National Institutes of Health (NIH) Grant 9P41GM104601 (K.S.), XSEDE Grant MCA93S028 (K.S.), NIH Grant PO1AI083222 (B.A.S.), NIH Grant RO1HL069031 (K.L.H.), The Max-Planck Society, and Marie Curie ITN FP7 Project CARMUSYS (PITN-GA-2008-213592) (P.H.S.).

Notes

The authors declare no competing financial interest.

ACKNOWLEDGMENTS

We thank Dr. Wei Han and Mr. Steven Wang for writing the interaction energy calculation program and Dr. Xueqing Zou for helpful discussions.

ABBREVIATIONS

Aichi, A/Aichi/68/H3N2; ASA, accessible surface area; CMAP, correction maps; CRD, carbohydrate recognition domain; HA, hemagglutinin; HTBE, human respiratory epithelial; IAV, influenza A virus; Man, D-mannose; Man9, methyl α-D-mannopyranosyl-(1R2)-α-D-mannopyranosyl-(1R2)-α-D-mannopyranosyl-(1R3)-[α-D-mannopyranosyl-(1R2)-α-D-mannopyranosyl-(1R3)-[α-D-mannopyranosyl-(1R2)-α-D-mannopyranosyl-(1R6)]-α-D-mannopyranosyl-(1R6)]-α-D-mannopyranoside; MDCK, Madin-Darby canine kidney; MD, molecular dynamics; Nag, *N*-acetylglucosamine; NCRD, neck and carbohydrate recognition domain; *NPT*, constant number of particle, pressure, and temperature; *NVT*, constant number of particle, volume, and temperature; Phil82, A/Philippines/1982/H3N2; PR8, A/Puerto Rico/8/1934/H1N1; rmsd, root-mean-square deviation; SA, sialic acid; SP-D, surfactant protein D; TLS, translation libration screw; VMD, Visual Molecular Dynamics; WT, wild-type human SP-D NCRD.

REFERENCES

(1) Ariki, S., Nishitani, C., and Kuroki, Y. (2012) Diverse functions of pulmonary collectins in host defense of the lung. *J. Biomed. Biotechnol. 2012*, e532071.

(2) Ng, W. C., Tate, M. D., Brooks, A. G., and Reading, P. C. (2012) Soluble host defense lectins in innate immunity to influenza virus. *J. Biomed. Biotechnol. 2012*, e732191.

(3) Chroneos, Z. C., Sever-Chroneos, Z., and Shepherd, V. L. (2010) Pulmonary surfactant: An immunological perspective. *Cell. Physiol. Biochem. 25*, 13−26.

(4) Nayak, A., Dodagatta-Marri, E., Tsolaki, A. G., and Kishore, U. (2012) An Insight into the Diverse Roles of Surfactant Proteins, SP-A and SP-D in Innate and Adaptive Immunity. *Front. Immunol. 3*, 131.

(5) Waters, P., Vaid, M., Kishore, U., and Madan, T. (2009) Lung surfactant proteins A and D as pattern recognition proteins. *Adv. Exp. Med. Biol. 653*, 74−97.

(6) Seaton, B. A., Crouch, E. C., McCormack, F. X., Head, J. F., Hartshorn, K. L., and Mendelsohn, R. (2010) Review: Structural determinants of pattern recognition by lung collectins. *Innate Immun. 16*, 143−150.

(7) Hartshorn, K. L., Crouch, E. C., White, M. R., Eggleton, P., Tauber, A. I., Chang, D., and Sastry, K. (1994) Evidence for a protective role of pulmonary surfactant protein D (SP-D) against influenza A viruses. *J. Clin. Invest. 94*, 311−319.

(8) Reading, P. C., Morey, L. S., Crouch, E. C., and Anders, E. M. (1997) Collectin-mediated antiviral host defense of the lung: Evidence from influenza virus infection of mice. *J. Virol. 71*, 8204−8212.

(9) Hartshorn, K. L., Webby, R., White, M. R., Tecle, T., Pan, C., Boucher, S., Moreland, R. J., Crouch, E. C., and Scheule, R. K. (2008) Role of viral hemagglutinin glycosylation in anti-influenza activities of recombinant surfactant protein D. *Respir. Res. 9*, 65.

(10) Hartshorn, K. L., White, M. R., Voelker, D. R., Coburn, J., Zaner, K., and Crouch, E. C. (2000) Mechanism of binding of surfactant protein D to influenza A viruses: Importance of binding to haemagglutinin to antiviral activity. *Biochem. J. 351* (Part 2), 449−458.

(11) LeVine, A. M., Whitsett, J. A., Hartshorn, K. L., Crouch, E. C., and Korfhagen, T. R. (2001) Surfactant protein D enhances clearance of influenza A virus from the lung in vivo. *J. Immunol. 167*, 5868−5873.

(12) Hawgood, S., Brown, C., Edmondson, J., Stumbaugh, A., Allen, L., Goerke, J., Clark, H., and Poulain, F. (2004) Pulmonary collectins modulate strain-specific influenza a virus infection and host responses. *J. Virol. 78*, 8565−8572.

(13) Vigerust, D. J., Ulett, K. B., Boyd, K. L., Madsen, J., Hawgood, S., and McCullers, J. A. (2007) N-linked glycosylation attenuates H3N2 influenza viruses. *J. Virol. 81*, 8593−8600.

(14) Qi, L., Kash, J. C., Dugan, V. G., Jagger, B. W., Lau, Y. F., Sheng, Z. M., Crouch, E. C., Hartshorn, K. L., and Taubenberger, J. K. (2011) The ability of pandemic influenza virus hemagglutinins to induce lower respiratory pathology is associated with decreased surfactant protein D binding. *Virology 412*, 426−434.

(15) Crouch, E., Hartshorn, K., Horlacher, T., McDonald, B., Smith, K., Cafarella, T., Seaton, B., Seeberger, P. H., and Head, J. (2009) Recognition of mannosylated ligands and influenza A virus by human surfactant protein D: Contributions of an extended site and residue 343. *Biochemistry 48*, 3335−3345.

(16) Crouch, E., Nikolaidis, N., McCormack, F., McDonald, B., Allen, K., Rynkiewicz, M., Cafarella, T., White, M., Lewnard, K., Leymarie, N., Zaia, J., Seaton, B., and Hartshorn, K. (2011) Mutagenesis of SP-D informed by evolution and X-ray crystallography enhances defenses against influenza A virus in vivo. *J. Biol. Chem. 286*, 40681−40692.

(17) Hartshorn, K. L., White, M. R., Tecle, T., Sorensen, G. L., Holmskov, U., and Crouch, E. C. (2010) Viral Aggregating and Opsonizing Activity in Collectin Trimers. *Am. J. Physiol. 298*, L79−L88.

(18) Ekiert, D. C., Bhabha, G., Elsliger, M. A., Friesen, R. H., Jongeneelen, M., Throsby, M., Goudsmit, J., and Wilson, I. A. (2009) Antibody recognition of a highly conserved influenza virus epitope. *Science 324*, 246−251.

(19) Fleury, D., Daniels, R. S., Skehel, J. J., Knossow, M., and Bizebard, T. (2000) Structural evidence for recognition of a single epitope by two distinct antibodies. *Proteins 40*, 572−578.

(20) Skehel, J. J., and Wiley, D. C. (2000) Receptor binding and membrane fusion in virus entry: The influenza hemagglutinin. *Annu. Rev. Biochem. 69*, 531−569.

(21) Sui, J., Hwang, W. C., Perez, S., Wei, G., Aird, D., Chen, L. M., Santelli, E., Stec, B., Cadwell, G., Ali, M., Wan, H., Murakami, A., Yammanuru, A., Han, T., Cox, N. J., Bankston, L. A., Donis, R. O., Liddington, R. C., and Marasco, W. A. (2009) Structural and functional bases for broad-spectrum neutralization of avian and human influenza A viruses. *Nat. Struct. Mol. Biol. 16*, 265−273.

(22) van Eijk, M., Rynkiewicz, M. J., White, M. R., Hartshorn, K. L., Zou, X., Schulten, K., Luo, D., Crouch, E. C., Cafarella, T. R., Head, J. F., Haagsman, H. P., and Seaton, B. A. (2012) A unique sugar-binding site mediates the distinct anti-influenza activity of pig surfactant protein D. *J. Biol. Chem. 287*, 26666−26677.

(23) Zhang, J., Zheng, Q., and Zhang, H. (2010) Insight into the dynamic interaction of different carbohydrates with human surfactant

protein D: Molecular dynamics simulations. *J. Phys. Chem. B 114*, 7383−7390.
(24) Mazumder, P., and Mukhopadhyay, C. (2012) Conformations, dynamics and interactions of di-, tri- and pentamannoside with mannose binding lectin: A molecular dynamics study. *Carbohydr. Res. 349*, 59−72.
(25) Guardia, C. M., Gauto, D. F., Di Lella, S., Rabinovich, G. A., Marti, M. A., and Estrin, D. A. (2011) An integrated computational analysis of the structure, dynamics, and ligand binding interactions of the human galectin network. *J. Chem. Inf. Model. 51*, 1918−1930.
(26) Yongye, A. B., Calle, L., Arda, A., Jimenez-Barbero, J., Andre, S., Gabius, H. J., Martinez-Mayorga, K., and Cudic, M. (2012) Molecular recognition of the Thomsen-Friedenreich antigen-threonine conjugate by adhesion/growth regulatory galectin-3: Nuclear magnetic resonance studies and molecular dynamics simulations. *Biochemistry 51*, 7278−7289.
(27) Priyadarzini, T. R., Selvin, J. F., Gromiha, M. M., Fukui, K., and Veluraja, K. (2012) Theoretical investigation on the binding specificity of sialyldisaccharides with hemagglutinins of influenza A virus by molecular dynamics simulations. *J. Biol. Chem. 287*, 34547−34557.
(28) Kasson, P. M., Ensign, D. L., and Pande, V. S. (2009) Combining molecular dynamics with bayesian analysis to predict and evaluate ligand-binding mutations in influenza hemagglutinin. *J. Am. Chem. Soc. 131*, 11338−11340.
(29) Xu, D., Newhouse, E. I., Amaro, R. E., Pao, H. C., Cheng, L. S., Markwick, P. R., McCammon, J. A., Li, W. W., and Arzberger, P. W. (2009) Distinct glycan topology for avian and human sialopentasaccharide receptor analogues upon binding different hemagglutinins: a molecular dynamics perspective. *J. Mol. Biol. 387*, 465−491.
(30) Crouch, E., Tu, Y., Briner, D., McDonald, B., Smith, K., Holmskov, U., and Hartshorn, K. (2005) Ligand specificity of human surfactant protein D: Expression of a mutant trimeric collectin that shows enhanced interactions with influenza A virus. *J. Biol. Chem. 280*, 17046−17056.
(31) Crouch, E. C., Smith, K., McDonald, B., Briner, D., Linders, B., McDonald, J., Holmskov, U., Head, J., and Hartshorn, K. (2006) Species differences in the carbohydrate binding preferences of surfactant protein D. *Am. J. Respir. Cell Mol. Biol. 35*, 84−94.
(32) Ratner, D. M., Plante, O. J., and Seeberger, P. H. (2002) A Linear Synthesis of Branched High-Mannose Oligosaccharides from the HIV-1 Viral Surface Envelope Glycoprotein gp120. *Eur. J. Org. Chem.*, 826−833.
(33) Grice, P., Ley, S. V., Pietruszka, J., and Priepke, H. W. M. (1996) Synthesis of the Nonamannan Residue of a Glycoprotein with High Mannose Content. *Angew. Chem., Int. Ed. 35*, 197−200.
(34) Otwinowski, Z., and Minor, W. (1997) *Methods Enzymol. 276*, 307−326.
(35) Adams, P. D., Afonine, P. V., Bunkoczi, G., Chen, V. B., Davis, I. W., Echols, N., Headd, J. J., Hung, L. W., Kapral, G. J., Grosse-Kunstleve, R. W., McCoy, A. J., Moriarty, N. W., Oeffner, R., Read, R. J., Richardson, D. C., Richardson, J. S., Terwilliger, T. C., and Zwart, P. H. (2010) PHENIX: A comprehensive Python-based system for macromolecular structure solution. *Acta Crystallogr. D66*, 213−221.
(36) Emsley, P., and Cowtan, K. (2004) Coot: Model-building tools for molecular graphics. *Acta Crystallogr. D60*, 2126−2132.
(37) Sauter, N. K., Hanson, J. E., Glick, G. D., Brown, J. H., Crowther, R. L., Park, S. J., Skehel, J. J., and Wiley, D. C. (1992) Binding of influenza virus hemagglutinin to analogs of its cell-surface receptor, sialic acid: Analysis by proton nuclear magnetic resonance spectroscopy and X-ray crystallography. *Biochemistry 31*, 9609−9621.
(38) Pejchal, R., Doores, K. J., Walker, L. M., Khayat, R., Huang, P. S., Wang, S. K., Stanfield, R. L., Julien, J. P., Ramos, A., Crispin, M., Depetris, R., Katpally, U., Marozsan, A., Cupo, A., Maloveste, S., Liu, Y., McBride, R., Ito, Y., Sanders, R. W., Ogohara, C., Paulson, J. C., Feizi, T., Scanlan, C. N., Wong, C. H., Moore, J. P., Olson, W. C., Ward, A. B., Poignard, P., Schief, W. R., Burton, D. R., and Wilson, I. A. (2011) A potent and broad neutralizing antibody recognizes and penetrates the HIV glycan shield. *Science 334*, 1097−1103.
(39) Frank, M., Lutteke, T., and von der Lieth, C. W. (2007) GlycoMapsDB: A database of the accessible conformational space of glycosidic linkages. *Nucleic Acids Res. 35*, 287−290.
(40) Shrive, A. K., Martin, C., Burns, I., Paterson, J. M., Martin, J. D., Townsend, J. P., Waters, P., Clark, H. W., Kishore, U., Reid, K. B., and Greenhough, T. J. (2009) Structural characterisation of ligand-binding determinants in human lung surfactant protein D: Influence of Asp325. *J. Mol. Biol. 394*, 776−788.
(41) Humphrey, W., Dalke, A., and Schulten, K. (1996) VMD: Visual molecular dynamics. *J. Mol. Graphics 14*, 27−38.
(42) Khubchandani, K. R., Oberley, R. E., and Snyder, J. M. (2001) Effects of surfactant protein A and NaCl concentration on the uptake of *Pseudomonas aeruginosa* by THP-1 cells. *Am. J. Respir. Cell Mol. Biol. 25*, 699−706.
(43) Zheng, H., Chruszcz, M., Lasota, P., Lebioda, L., and Minor, W. (2008) Data mining of metal ion environments present in protein structures. *J. Inorg. Biochem. 102*, 1765−1776.
(44) Weigel, P. H. (1980) Characterization of the asialoglycoprotein receptor on isolated rat hepatocytes. *J. Biol. Chem. 255*, 6111−6120.
(45) Phillips, J. C., Braun, R., Wang, W., Gumbart, J., Tajkhorshid, E., Villa, E., Chipot, C., Skeel, R. D., Kale, L., and Schulten, K. (2005) Scalable molecular dynamics with NAMD. *J. Comput. Chem. 26*, 1781−1802.
(46) Mackerell, A. D., Jr., Feig, M., and Brooks, C. L., III (2004) Extending the treatment of backbone energetics in protein force fields: Limitations of gas-phase quantum mechanics in reproducing protein conformational distributions in molecular dynamics simulations. *J. Comput. Chem. 25*, 1400−1415.
(47) Jorgensen, W. L., Chandrasekhar, J., Madura, J. D., Impey, R. W., and Klein, M. L. (1983) Comparison of simple potential functions for simulating liquid water. *J. Chem. Phys. 79*, 926−935.
(48) Guvench, O., Greene, S. N., Kamath, G., Brady, J. W., Venable, R. M., Pastor, R. W., and Mackerell, A. D., Jr. (2008) Additive empirical force field for hexopyranose monosaccharides. *J. Comput. Chem. 29*, 2543−2564.
(49) Guvench, O., Hatcher, E. R., Venable, R. M., Pastor, R. W., and Mackerell, A. D. (2009) CHARMM Additive All-Atom Force Field for Glycosidic Linkages between Hexopyranoses. *J. Chem. Theory Comput. 5*, 2353−2370.
(50) Martyna, G. J., Tobias, D. J., and Klein, M. L. (1994) Constant pressure molecular dynamics algorithms. *J. Chem. Phys. 101*, 4177−4189.
(51) Onufriev, A., Bashford, D., and Case, D. A. (2004) Exploring protein native states and large-scale conformational changes with a modified generalized born model. *Proteins 55*, 383−294.
(52) Wang, L., Friesner, R. A., and Berne, B. J. (2010) Hydrophobic interactions in model enclosures from small to large length scales: Non-additivity in explicit and implicit solvent models. *Faraday Discuss. 146*, 283−298 , 395−401.
(53) Shrake, A., and Rupley, J. A. (1973) Environment and exposure to solvent of protein atoms. Lysozyme and insulin. *J. Mol. Biol. 79*, 351−371.
(54) Gonzalez, L., Bruix, M., Diaz-Maurino, T., Feizi, T., Rico, M., Solis, D., and Jimenez-Barbero, J. (2000) Conformational studies of the Man8 oligosaccharide on native ribonuclease B and on the reduced and denatured protein. *Arch. Biochem. Biophys. 383*, 17−27.
(55) Woods, R. J., Pathiaseril, A., Wormald, M. R., Edge, C. J., and Dwek, R. A. (1998) The high degree of internal flexibility observed for an oligomannose oligosaccharide does not alter the overall topology of the molecule. *Eur. J. Biochem. 258*, 372−386.
(56) Petrescu, A. J., Milac, A. L., Petrescu, S. M., Dwek, R. A., and Wormald, M. R. (2004) Statistical analysis of the protein environment of N-glycosylation sites: Implications for occupancy, structure, and folding. *Glycobiology 14*, 103−114.
(57) Jo, S., Lee, H. S., Skolnick, J., and Im, W. (2013) Restricted N-glycan conformational space in the PDB and its implication in glycan structure modeling. *PLoS Comput. Biol. 9*, e1002946.

(58) Petrescu, A. J., Petrescu, S. M., Dwek, R. A., and Wormald, M. R. (1999) A statistical analysis of N- and O-glycan linkage conformations from crystallographic data. *Glycobiology 9*, 343−352.
(59) Weis, W. I., Drickamer, K., and Hendrickson, W. A. (1992) Structure of a C-type mannose-binding protein complexed with an oligosaccharide. *Nature 360*, 127−134.
(60) Ng, K. K., Kolatkar, A. R., Park-Snyder, S., Feinberg, H., Clark, D. A., Drickamer, K., and Weis, W. I. (2002) Orientation of bound ligands in mannose-binding proteins. Implications for multivalent ligand recognition. *J. Biol. Chem. 277*, 16088−16095.
(61) Jain, N. U., Noble, S., and Prestegard, J. H. (2003) Structural characterization of a mannose-binding protein-trimannoside complex using residual dipolar couplings. *J. Mol. Biol. 328*, 451−462.
(62) Sayers, E. W., and Prestegard, J. H. (2002) Conformation of a trimannoside bound to mannose-binding protein by nuclear magnetic resonance and molecular dynamics simulations. *Biophys. J. 82*, 2683−2699.
(63) Iobst, S. T., Wormald, M. R., Weis, W. I., Dwek, R. A., and Drickamer, K. (1994) Binding of sugar ligands to Ca^{2+}-dependent animal lectins. I. Analysis of mannose binding by site-directed mutagenesis and NMR. *J. Biol. Chem. 269*, 15505−15511.
(64) Feinberg, H., Mitchell, D. A., Drickamer, K., and Weis, W. I. (2001) Structural basis for selective recognition of oligosaccharides by DC-SIGN and DC-SIGNR. *Science 294*, 2163−2166.
(65) Guo, Y., Feinberg, H., Conroy, E., Mitchell, D. A., Alvarez, R., Blixt, O., Taylor, M. E., Weis, W. I., and Drickamer, K. (2004) Structural basis for distinct ligand-binding and targeting properties of the receptors DC-SIGN and DC-SIGNR. *Nat. Struct. Mol. Biol. 11*, 591−598.
(66) Feinberg, H., Castelli, R., Drickamer, K., Seeberger, P. H., and Weis, W. I. (2007) Multiple modes of binding enhance the affinity of DC-SIGN for high mannose N-linked glycans found on viral glycoproteins. *J. Biol. Chem. 282*, 4202−4209.
(67) Mari, S., Serrano-Gomez, D., Canada, F. J., Corbi, A. L., and Jimenez-Barbero, J. (2004) 1D saturation transfer difference NMR experiments on living cells: The DC-SIGN/oligomannose interaction. *Angew. Chem., Int. Ed. 44*, 296−298.
(68) Reina, J. J., Diaz, I., Nieto, P. M., Campillo, N. E., Paez, J. A., Tabarani, G., Fieschi, F., and Rojo, J. (2008) Docking, synthesis, and NMR studies of mannosyl trisaccharide ligands for DC-SIGN lectin. *Org. Biomol. Chem. 6*, 2743−2754.
(69) van Eijk, M., Haagsman, H. P., Skinner, T., Archibald, A., Reid, K. B., and Lawson, P. R. (2000) Porcine lung surfactant protein D: Complementary DNA cloning, chromosomal localization, and tissue distribution. *J. Immunol. 164*, 1442−1450.
(70) Hartshorn, K. L., White, M. R., Smith, K., Sorensen, G., Kuroki, Y., Holmskov, U., Head, J., and Crouch, E. C. (2010) Increasing antiviral activity of surfactant protein d trimers by introducing residues from bovine serum collectins: Dissociation of mannan-binding and antiviral activity. *Scand. J. Immunol. 72*, 22−30.